Analysis of Composite Truss-core Sandwich Panels for Thermal Protection Systems

Pires, M.
Guarulhos University
Av. Anton Philips, n° 1, Vila Hermínia
Guarulhos / SP CEP: 07030-010

Abstract

The focus this paper was develop an analytical method to predict the thermal force resultants and moments of an orthotropic integral thermal protection system sandwich panel composed of four composite laminates. Determination of thermal stresses in the face sheets and the web caused by temperature variation. The method was demonstrated by calculating stresses in a sandwich panel subjected to a temperature distribution described by a polynomial in the thickness direction. The results for stresses are compared with that from a 3-D FEM analysis volume element of the sandwich structure, and the comparison was found to be within 6% difference.

Nomenclature

2a	=	unit cell length
$\{D\}^{(e)}$	=	deformation vector of the *e*th component (microdeformation)
$\{D\}^{(M)}$	=	deformation vector of the unit cell (macrodeformation)
e_{ms}	=	bottom face sheet thickness
e_{mi}	=	top face sheet thickness
e_n	=	web thickness
$F_i^{(m)}$	=	nodal force on the finite element method model
f	=	web length
h	=	height of the sandwich panel (centerline to centerline)
i	=	component index of the corrugated core
l	=	length of the cantilever beam
Q_{ij}	=	transformed lamina stiffness matrix
Qx, Qy	=	shear force on the unit cells
$[T_D]^{(e)}$	=	deformation transformation matrix of the *i*th component of the corrugated core
U	=	unit cell strain energy
$\bar{y}$	=	local axis of the web
ΔT	=	temperature distribution in the integral thermal protection system
ε_0	=	midplane strain
θ	=	angle of web inclination
k	=	curvature
$\tau_{x\bar{y}}$	=	local shear stress in the webs

1. Introduction

Thermal structural challenges can be quite severe on aerospatial vehicles. One of the primary thermal structural challenges results from large thermal gradients. Thermal protection systems (TPS) are the key features incorporated into a spacecraft's design to protect it from severe aerodynamic heating during high speed travel through planetary atmospheres. The thermal protection system is the key technology that enables a spacecraft to be fully reusable, lightweight and easily maintainable. Add on TPS concepts have been used since the beginning of the space race. Metallic thermal protection systems are a key technology that may help achieve the goal of reducing the cost of space access. The inherent ductility and design flexibility of metal TPS offer the potential for a more robust system with lower maintenance costs than competing systems. The foil-gage construction of current metallic TPS concepts makes it simple to improve durability by increasing the thickness of the outer face sheet to meet robustness

requirements.The Apollo space capsule used ablative TPS and the Space Shuttle Orbiter TPS technology consisted of ceramic tiles and blankets. Many problems arose from the add on concept such as incompatibility, high maintenance costs, non load bearing, and not being robust and operable. To make the spacecraft's TPS more reliable, robust, and efficient, we investigated Integral Thermal Protection System (ITPS) concept in which the load bearing structure and the TPS are combined into one single component. The design of an ITPS was a challenging task, because the requirement of a load bearing structure and a TPS are often conflicting. Finite element (FE) analysis is often the preferred method of choice for a structural analysis problem. However, as the structure becomes complex, the computational time and effort for an FE analysis increases. New structural analytical tools were developed, or available ones were modified, to perform a full structural analysis of the ITPS. With analytical tools, the designer is capable of obtaining quick and accurate results and has a good idea of the response of the structure without having to go to an FE analysis. A MATLAB ® code was developed to analytically determine performance metrics of the ITPS such as stresses, buckling, deflection, and other failure modes. The analytical models provide fast and accurate results that were within 6% difference from the FEM results. The optimization procedure usually performs 120 function evaluations for every design variable. Using the analytical models in the optimization procedure was a time saver, because the optimization time to reach an optimum design was reached in less than an hour, where as an FE optimization study would take hours to reach an optimum design. Corrugatedcore structures were designed for ITPS applications with loads and boundary conditions similar to that of a Space Shuttle like vehicle. Temperature, buckling, deflection and stress constraints were considered for the design and optimization process was achieved with consideration of all the constraints.

II. Geometric ITPS

Consider a simplified geometry of an ITPS unit cell shown in Fig. 1. The *z* axis is in the thickness direction of the ITPS panel. The stiffer longitudinal direction is parallel to the *x* axis, and *y* axis is in the transverse direction. The unit cell consists of two inclined webs and two thin face sheets. The unit cell is symmetric with respect to the *yz* plane. The upper face plate thickness e_{ms} can be different from the lower plate thickness e_{mi}, as well as the web thickness e_w. The unit cell can be identified by six geometric parameters *a; h;* e_{ms}*;* $e_{mi;}$ e_n*;* (Fig. 1). Four other dimensions b_c*;* d_c*; s;f* are obtained from geometric considerations. The equations for these relationships are as follows:

$$d = h - \frac{1}{2}e_{ms} - \frac{1}{2}e_{mi} \tag{1a}$$

$$f = \frac{1}{2}(a - \frac{d}{\tan\theta}) \tag{1b}$$

$$b = a - 2c \tag{1c}$$

$$f = \sqrt{d^2 + b^2} = \frac{d}{\sin\theta} = \frac{b}{\cos\theta} \tag{1d}$$

The ratio $c/a = 0$ corresponds to a triangular corrugated core, and $c/a = 0.5$ corresponds to a rectangular core.

III. Analytical Approach

Thermal and structural numerical analyses are required to develop the specific loading conditions from the trajectory information, to size the various components of the TPS panels and to calculate the response of the panels, in detail, to various thermal and mechanical loads. The generation of specific loading conditions and the thermal and structural sizing of various TPS panel components were performed in an iterative manner to arrive at the final panel dimensions. Micromechanical analysis of a unit cell was performed to determine the structure's extensional, bending, coupling shear stiffness, stresses, and unit cell behavior. Microscale stresses are the local facesheet and web stresses of the ITPS. The microscale stresses within the unit cell were computed using the micromechanical analysis. The relationship between the unit cell macrostress and macrostrains provided the constitutive relations for the material. Thus, constitutive characterization matrices [*A*], [*B*], [*D*] were found

directly from micromechanics. The stresses were also used to predict the failure of the corrugated core. A detailed formulation and description of the extensional, coupling, bending, and shearing stiffness of the ITPS panelThe finite element method was used to determine the response of a sandwich structure. However, a full 3-D finite element analysis is not economical to conduct a preliminary analysis. The number of nodes and elements needed to properly model the structure was excessive; Such panels may also be represented as a thick plate that is continuous, orthotropic, and homogenous, for which analytical and 2-D finite element method (FEM) solutions [1] are available. The computational time and effort in determining stiffness and thermal behavior of the ITPS is significantly reduced

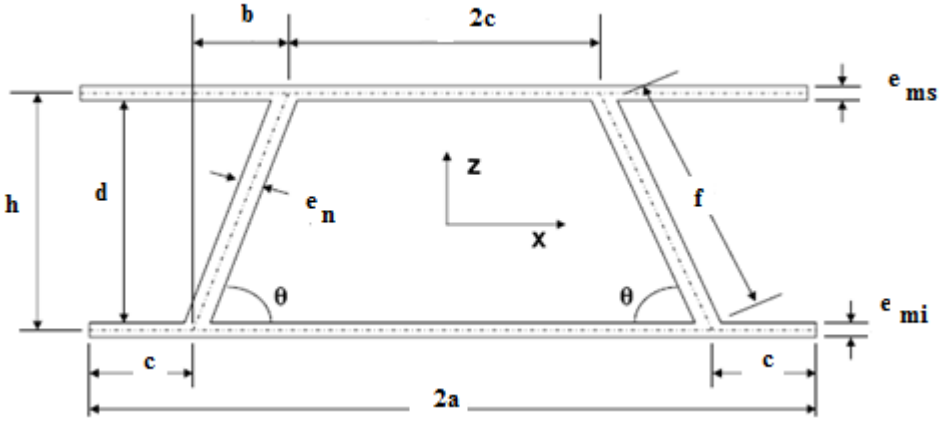

Fig. 1 Dimensions of the unit cell

in comparison with FEM. Analytical models have been proven to be fast, accurate. [2] used 3-D finite element (FE) analysis of the ITPS in developing response surfaces for optimization. The analytical models are able to provide the designer with an accurate description of the behavior of the ITPS when subjected to realistic reentry temperatures. The thermal moments and force resultants could cause the panel to thermally deflect, buckle, and yield. A TPS must be constrained from deflection to prevent local aerodynamic heating due to the change in the aerodynamic profile. Local buckling is an important design driver of an ITPS because of the thin webs and faces. The ITPS may be represented as an equivalent thick plate that is continuous, homogenous, and orthotropic with respect to the *x* and *y* directions. In the derivation of the stiffness parameters the following assumptions were made:
1) The deformation of the panel is less than 7% when compared with the panel thickness.
2) The panel dimensions in the *y* direction are 3–6 times larger than the unit-cell width 2*a*.
3) The face sheets are thin with respect to the core thickness.
4) The core contributes to bending stiffness in and about the *x* axis but not about the *y* axis.
5) The face and web plate laminates are symmetric with respect to their own midplane.
6) The core is sufficiently stiff so that the elastic modulus in the *z* direction is assumed to be infinite for the equivalent plate. Local buckling of the facing plates does not occur and the overall thickness of the panel is constant.

Researchers adopted these assumptions in the derivation of stiffness parameters of sandwich panels with corrugated core (Fung et. al. [3], Libove and Hubka *C* core[4]. The in-plane and out-of-plane stiffness governing the elastic response of a shear-deformable sandwich panel are defined in the context of laminated plate theory incorporating first-order shear deformable plate theory described by Vinson [5] and Whitney [6]. The appropriate stiffness of the orthotropic plate may be obtained by comparing the behavior of a unit cell of the corrugated-core sandwich panel with that of an element of the idealized homogeneous orthotropic plate (Fig. 2).

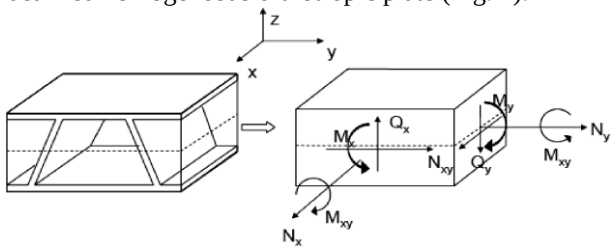

Fig. 2 Equivalent Orthotropic Thick Plate for the Unit-Cell Sandwich Panel

The in-plane extensional and shear response and out-of-plane (transverse) shear response of an orthotropic panel are governed by the following constitutive relation:

$$\begin{bmatrix} N_x \\ N_y \\ Q_y \\ Q_x \\ N_{xy} \\ M_x \\ M_y \\ M_{xy} \end{bmatrix} = \begin{bmatrix} A_{11} & A_{12} & 0 & 0 & 0 & 0 & 0 & 0 \\ A_{12} & A_{22} & 0 & 0 & 0 & 0 & 0 & 0 \\ 0 & 0 & A_{44} & 0 & 0 & 0 & 0 & 0 \\ 0 & 0 & 0 & A_{55} & 0 & 0 & 0 & 0 \\ 0 & 0 & 0 & 0 & A_{66} & 0 & 0 & 0 \\ 0 & 0 & 0 & 0 & 0 & D_{11} & D_{12} & 0 \\ 0 & 0 & 0 & 0 & 0 & D_{12} & D_{22} & 0 \\ 0 & 0 & 0 & 0 & 0 & 0 & 0 & D_{66} \end{bmatrix} \begin{Bmatrix} \varepsilon_{xo} \\ \varepsilon_{yo} \\ \gamma_{yz} \\ \gamma_{xz} \\ \gamma_{xyo} \\ \kappa_x \\ \kappa_y \\ \kappa_{xy} \end{Bmatrix} \tag{2}$$

$$\{F\} = [k]\{D\}$$

Eq. (2), ε and γ are the normal and shear strains, is k the bending and twisting curvatures, [A], [C] and [D} are the extensional, shear, and bending stiffness. The orthotropic plate is assumed to be symmetric.

3.1 Extensional, Bending, Coupling, and Transverse Shearing Stiffness

Consider a composite corrugated-core unit cell. The unit cell is composed of four components (two faces and two webs), each with its own material properties and ABD matrix; the ABD matrix is composed of three matrices: A is the extensional stiffness matrix, B is the coupling stiffness matrix, and D is the bending stiffness matrix. The ABD matrix of each unit-cell component is combined together in an appropriate manner to create an overall stiffness of the ITPS sandwich panel. The analytical procedure of determining the overall stiffness of the ITPS sandwich panel has been discussed and determined by Martinez et al. [7]. Here is provide a brief description of the analytical method. The overall stiffness of the unit cell was determined by imposing unit midplane strains and curvature (macrodeformation) to the unit cell and then calculating the corresponding midplane strains and curvatures (microdeformations) in each component. The unit-cell components are the two face sheets and two webs. Transformation matrices that relate the macro and microdeformations were derived in the form

$$\{D\}^i = [T_D]^i \{D\}^M \tag{3}$$

In Eq. (3), $T^{(i)}_D$ is the deformation transformation matrix that relates macrodeformations to microdeformation, is $\{D\}^{(i)}$ the microdeformation in each component, and $D\}^{(M)}$ is the macrodeformation in the unit cell (refer to for the transformation matrix), and i = 1- 4, (1 = top face sheet, 2 = bottom face sheet, 3 = left web, 4= right web). Using the transformation matrices, the strain energy of each component was determined and added to determine the overall unit cell strain energy.

$$U^i = \frac{1}{2}(2a)\int_0^s \left(T_D^i\right)^T \{D^M\}^T K^i \left(T_D^i\right)\{D\}^M \, d\bar{y} \tag{4}$$

$$U^M = \frac{1}{2}(2a)^2 \left(\{D\}^M\right)^T [K]\{D\}^M = \sum_{i=1}^{4} \overline{U}^{(i)} \tag{5}$$

From the strain energy we determined the ITPS sandwich panel stiffness as the sum of the transformed stiffnesses of the components. The details of the derivation and verification of the method using fullscale finite element models are described in Martinez et al. [7].

$$K = \sum_{i=1}^{4} K^{(s)} \tag{6}$$

3.2 Heat Transfer and Temperature Distribution

Thermal analysis of an ITPS involves complex heat transfer mechanisms in severe transient thermal environments. Pressure, conduction, radiation, convection, and temperature variation all play important roles in the thermal performance of an ITPS Blosser [8]. The proposed ITPS is a multifunctional structure that possesses load-bearing capabilities as well as provides insulation for the space vehicle. During reentry the outer surface of the space vehicle is exposed to extreme reentry temperatures due to the incoming heat flux (see Fig. 3).

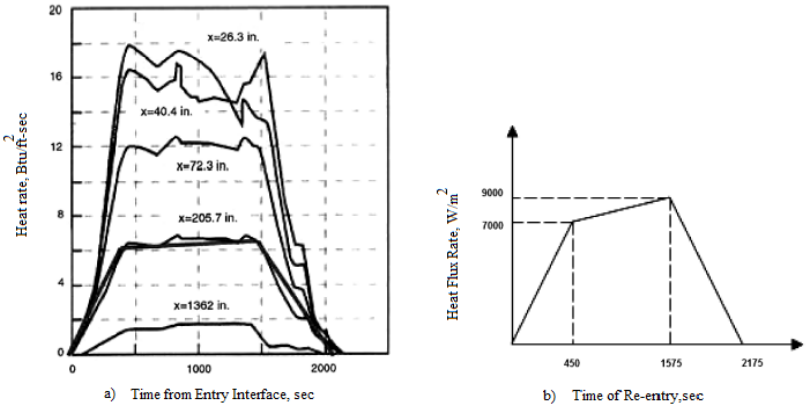

Fig. 3 Heating Profiles for a Shuttle-like vehicle obtained from Dorsey et al. [9] a) during Reentry on Vehicle Windward Centerline, and b) Heating Rate used for Preliminary Analysis

The heat flux causes the ITPS temperature to rise dramatically, and as a result it causes severe thermal stresses that lead to excessive thermal deflection and even thermal buckling. Knowing the response of the ITPS to a change in temperature is a critical need because panel deflection, buckling (local or global), temperature, and yielding are all critical functions of an ITPS that influence the design. Consider an orthotropic unit cell of the ITPS with the following dimensions: : a = 60 mm, h = 120 mm, e_{ms} = 1.5mm, e_n = 1.5 mm, $\theta = 65^o$, subjected to an incident heat flux versus reentry time of a Space Shuttle-like vehicle (Fig. 4). The corrugated core sandwich panel is assumed to be made out of graphite/epoxy AS/3501, $E1$ = 140 GPa, $E2$ = 8 GPa, $G12$ = 7 GPa, =14, $\upsilon = 0.3$, with four laminas in each component and a stacking sequence of [90/0]s. Each temperature distribution resulted in thermal force resultants and thermal moments that caused the sandwich structure to linearly deform. . Therefore, a micromechanics (homogenization) approach was used to determine the unit-cell thermal forces and moments. Consider the thermoelastic laminate constitutive relation

$$\begin{Bmatrix} N \\ M \end{Bmatrix} = [K] \begin{Bmatrix} \varepsilon_0 \\ K \end{Bmatrix} - \begin{bmatrix} N^T \\ M^T \end{bmatrix} \tag{8}$$

In Eq. (8), N^T and M^T are the unit cell's thermal force resultant and moment due to a temperature change of the ITPS. The thermal force resultants and moments are equal to the negative of forces and moments that act on the unit cell when it is completely constrained at its lateral boundary surfaces. An analytical procedure for predicting the ITPS thermal force and moment resultants are presented in this paper.

3.3 Thermal Force Resultants and Moments

An analytical method was developed to predict the thermal force and moment resultants acting on an ITPS sandwich panel from a given temperature distribution. Consider a unit cell made up of four composite laminates (two face sheets and two webs). Each laminate has its respective material properties and stiffness matrix. The unit cell was

subjected to a temperature distribution $\Delta T(\bar{y})$ where $\bar{y}$ was the local axis of the inclined web starting from the top face. The temperature distribution equation was determined by fitting a quartic polynomial to the temperature distribution shown in Fig. 4.

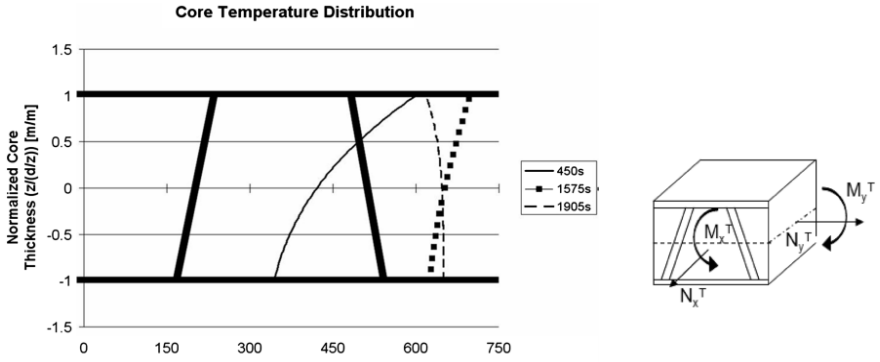

Figure 4 Core temperature distribution at three reentry times, and resulting thermal force resultants and thermal moments

A reference temperature at which the laminate is stress-free was assumed to be at room temperature and the temperatures in the faces were considered to be constant because the faces are thin when compared with the ITPS core thickness. Because of symmetry only half the unit cell was analyzed. The half-unit cell was constrained to prevent displacement in the *x* and *y* directions. The top face sheet had roller support in the *z* direction, which allowed the webs to expand in the d $\bar{y}$ direction (Fig. 5).

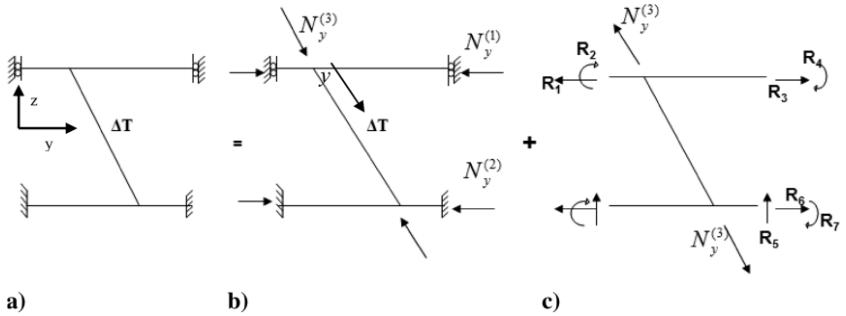

Figure 5 Half-unit cell of the corrugated-core sandwich panel with a temperature distribution, b) constrained thermal problem, and c) unconstrained relaxed expansion

The thermal problem was broken down into two problems. The first problem was the constrained problem in which force resultants that are equal and opposite to the component's (face or web) thermal forces were applied to the unit cell, This behavior is given by

$$\left[N_i\right]^{(e)} = \left[\overline{A}\,\overline{B}\,\overline{D}\right]\{0\} - \frac{1}{L}\int_{-\frac{s}{2}}^{\frac{s}{2}} \left(Q_{ij}^{e}\right)_k \left(z_k - z_{k-1}\right)\Delta T(\bar{y})\,d\bar{y} \tag{9}$$

The equal and opposite forces prevent any expansion in the half unit cell; hence the strains are equal to zero. The average thermal force resultants were determined for the webs because the temperature distribution had a polynomial variation. The second problem is an unconstrained half-unit cell with no temperature distribution, and the forces developed in the constrained problem, $N_y^{(1)}$, $N_y^{(2)}$, and $N_y^{(3)}$ are relaxed. The relaxed force resultants are equal and opposite to the force resultants obtained in Eq. (9). The constraints are represented by the reactions shown in Fig. 5c. The constraints are unknown reaction forces that were determined by Castigliano's second theorem [10]. The strain energy due to bending and normal force was considered. The strain energy of each component was determined and then summed to obtain the total strain energy in the half-unit cell. There are seven unknown reactions to be determined. To determine the seven unknown reactions seven boundary conditions were imposed, which are that the

displacement and rotations due to each reaction are zero. The seven boundary conditions along with Castigliano's second theorem lead to a system of seven linear equations with seven unknowns:

$$\frac{\partial U_s}{\partial R_i} = 0 \qquad \text{i= 1, 2, 3,….7}$$

(10)

Solving Eq. (11) leads to the solution of the seven reaction forces. By summing the *x* and *y* forces in Fig. 6c along with the *x*- and *y*-force resultant results from Fig. 6b, the desired thermal force resultant and moment for an ITPS sandwich panel were obtained. The relevant equations are given as follows:

$$\mathrm{N_y} = \mathrm{R_3} + \mathrm{R_6} + (\mathrm{N_y^{(1)}} + \mathrm{N_y^{(2)}})$$

(11)

$$\mathrm{M_y} = \mathrm{R_4} + \mathrm{R_7} + \frac{\mathrm{d}}{2}(\mathrm{N_y^{(1)}} - \mathrm{N_y^2}) + \frac{\mathrm{d}}{2}(\mathrm{R_6} - \mathrm{R_3})$$

(12)

$$N_x = \frac{1}{2a}(N_x^{(1)} 2a + N_x^{(2)} 2a + N_x^{(3)} 2s)$$

(13)

$$\mathrm{M_x} = \left[\frac{\mathrm{d}}{2}\left(\mathrm{N_x^{(1)}} - \mathrm{N_x^{(2)}}\right)2\mathrm{a} + \sum_{\mathrm{i=1}}^{\mathrm{N}} 2(\mathrm{Z_i} - \frac{\mathrm{d}}{2})\mathrm{N_x^{(3)}}(\mathrm{i})(\frac{\mathrm{s}}{\mathrm{N}})\right]\frac{1}{2\mathrm{a}}$$

(14)

In Eq. (14), *N* is the number of discretization points in the web length. The force and moments resultants that are needed to constrain the unit cell during a change in temperature is equal to the negative of the thermal force resultants and moments of the ITPS as shown in Eq. (15)

$$\left[\mathrm{N^T}, \mathrm{M^T}\right] = \left[-\mathrm{N}, -\mathrm{M}\right]$$

(15)

3.5 Thermal Stress in the Faces and Webs

The analytical procedure was extended to obtain the thermal stresses in each component due to a given through-the-thickness temperature variation. According to classical laminate plate theory, the equations needed to determine thermal stresses are:

$$\sigma = \left[\overline{\mathrm{Q}}\right](\varepsilon - \alpha\Delta\mathrm{T})$$

(16)

To determine the thermal stresses in either the faces or the webs, the microthermal deformation of each component due to a unit-cell macrostrain or curvature must be known. The microdeformation of each component was determined by Eq. (3), which relates macro to microdeformation. The deformation transformation matrices that were derived by Martinez et al. [7] were used to determine microstrains and curvatures in the faces and webs (see for the transformation deformation matrices).

1. Microthermal Stresses, Constrained Case

The thermal stresses in the faces and webs were derived for an ITPS unit cell. The first case that was investigated was the constrained case where strains in the *x* and *y* directions were zero, however, the webs were free to expand in the web length direction and constrained in the *x* direction. The thermal stress equation for the constrained thermal expansion problem is shown in the following equation:

$$\sigma = \left[\overline{\mathrm{Q}}\right]\{\alpha\}\Delta\mathrm{T}\left(\frac{-\mathrm{h}}{2}, \frac{\mathrm{h}}{2}\right)$$

(17)

Equation (17) is only valid for the top and bottom face sheets because the faces are fully constrained and the strains are zero. The webs, however, were not fully constrained and were allowed to expand in the $\bar{y}$ direction only. Therefore, an analytical solution for the web expansion under a fourth-order polynomial temperature distribution was derived. From Fig. 5a it can be seen that the constrained thermal problem for the half-unit cell was broken down into two individual problems. Problem 1 is Fig. 5b and problem 2 is Fig. 5c. The web strains in the $\bar{y}$ direction for problem one and problem two were determined and then summed to obtain the total web strain for the constrained thermal problem, which took into account the web expansion. The web strain from problem-2 was obtained by determining the midplane strains and curvatures in the webs due to the reactions and relaxed forces (Fig. 6).

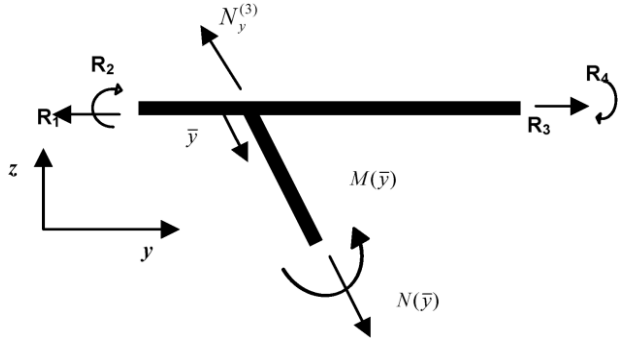

Figure 6 Free body diagram of the top face sheet and web.

By summing the forces and moments in the $\bar{y}$ direction the equation that characterizes the force and moment at any location on the web was determined (refer to for the force and moment equation on the web). The midplane strain and curvature in the webs were determined by multiplying the force vector of the web with the inverse of the web's stiffness matrix, Eqs. (18) and (19)

$$\begin{Bmatrix} 0 \\ \varepsilon_{\bar{y}0} \\ 0 \\ 0 \\ K_{\bar{y}} \\ 0 \end{Bmatrix} = \begin{bmatrix} \overline{A}\,\overline{B} \\ \overline{B}\,\overline{D} \end{bmatrix}^{-1(nerv)} \begin{Bmatrix} N_x \\ N_y \\ N_{xy} \\ M_x \\ M_y \\ Mxy \end{Bmatrix} \tag{18}$$

$$\varepsilon_{\bar{y}0}(\bar{y}) = \left(\frac{-\mathrm{A}_{12}^{*2}}{\mathrm{A}_{11}^{*}} + \mathrm{A}_{22}^{*}\right)\mathrm{N}(\bar{y}) \tag{19}$$

$$k_{\bar{y}}(\bar{y}) = \left(\frac{D_{12}^{*2}}{D_{11}^{*}} + D_{22}^{*}\right) \tag{20}$$

The web strain for problem-1 was determined by first modeling the free body diagram of the web only from Fig. 6b. The webs are constrained by a compressive force from Eq. (9), which was the average force needed to constrain theweb in the web length direction. However, the average displacement was zero, but the local displacements and local strains were not zero because of the fourth order polynomial of the temperature distribution, which causes localthermal strains. An analytical equation was derived that accounts for the expansion of the web due to a temperature distribution through the web length. Considering only the $\bar{y}$ direction, which accounts for web length expansion from Fig. 7, and using the constitutive relation results in the following equation:

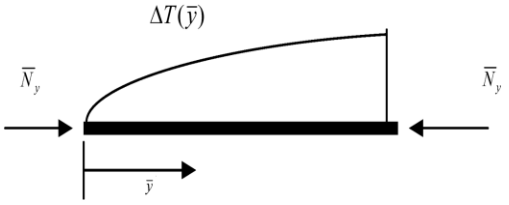

Figure 7 Diagram of the Webs with an Average Constraining Force and a Quartic Temperature Distribution.

$$\overline{\mathrm{N}}_{\bar{\mathrm{y}}} = \overline{\mathrm{A}}_{22}\varepsilon_{\mathrm{y0}} - \hat{\mathrm{N}}\Delta\mathrm{T}(\bar{\mathrm{y}}) \tag{21}$$

The differential equation of equilibrium for Fig. 7 is

$$\frac{\partial \overline{\mathrm{N}}_{\mathrm{xy}}}{\partial \bar{\mathrm{x}}} + \frac{\partial \overline{\mathrm{N}}_{\mathrm{y}}}{\partial \bar{\mathrm{y}}} = 0 \tag{22}$$

Substituting Eq. (21) into Eq. (22) results

$$\overline{A}_{22}\frac{\partial^2 \bar{\upsilon}}{\partial \bar{y}^2} - \hat{N}\frac{\partial}{\partial \bar{y}}\Delta T(\bar{y}) = 0 \tag{23}$$

Integrating Eq. (23) twice with respect to $\bar{y}$, the web displacement as a function of $\bar{y}$ was obtained

$$\bar{\upsilon}(\bar{\mathrm{y}}) = \iint \frac{\mathrm{N}}{\overline{\mathrm{A}}_{22}}\frac{\partial}{\partial \bar{\mathrm{y}}}\Delta\mathrm{T}(\bar{\mathrm{y}})\mathrm{d}\bar{\mathrm{y}}\mathrm{d}\bar{\mathrm{y}} + \mathrm{D}\bar{\mathrm{y}} + \mathrm{E} \tag{24}$$

Equation (24) has two unknown constants that were solved by considering two boundary conditions

$$\bar{\upsilon}(0) = 0 \qquad \bar{\upsilon}(s) = 0 \tag{25}$$

Substituting Eq. (24) into Eq. (25) and solving for the system of linear equations, the unknown constants *D* and *E* were determined. Finally, taking the partial derivative of Eq. (25) with respect to $\bar{y}$, the web midplane strain in the $\bar{y}$ direction for problem-1 was obtained

$$\varepsilon_{y0}(\bar{y}) = \frac{\partial}{\partial \bar{\mathrm{y}}}\bar{\upsilon}(\bar{\mathrm{y}}) = \frac{\partial}{\partial \bar{y}}\left[\iint \frac{\hat{\mathrm{N}}}{\overline{\mathrm{A}}_{22}}\frac{\partial}{\partial \bar{\mathrm{y}}}\Delta\mathrm{T}(\bar{\mathrm{y}})\mathrm{d}\bar{\mathrm{y}}\mathrm{d}\bar{\mathrm{y}} + \mathrm{D}\bar{\mathrm{y}} + \mathrm{E}\right] \tag{26}$$

Summing the strain obtained from Eqs. (19) and (26) yields the web strain in the web length direction for the constrained problem with consideration of web expansion.

2. Thermal Stresses, Unconstrained Case

In this section the stresses in the faces and webs due to the force resultants obtained from Eqs. (12–15) were determined. Using the thermal force vector from Eq. (16) and multiplying the result with the unit-cell stiffness, Eq. (7) yields the thermal strain and curvature for the unit cell

$$\begin{Bmatrix} \varepsilon_0 \\ \mathrm{K} \end{Bmatrix}^{\mathrm{M}} = \left[\mathrm{K}^{-1}\right]\begin{Bmatrix} -\mathrm{N} \\ -\mathrm{M} \end{Bmatrix} \tag{27}$$

Equation (27) solves the unit-cell strain and curvature under thermal loading. Using the result in Eq. (27) along with the deformation transformation matrix for the faces and the refined web stress deformation transformation matrix [16], the microdeformation of the faces and webs was determined, Eq. (2). The microdeformations are the local strains and curvature that the faces or the webs will undergo due to the temperature distribution. The face and web stresses were determined by multiplying the microdeformation from Eq. (27) with its respective transformed lamina stiffness matrix

$$[\sigma]^{(e)} = [\overline{Q}]^{(e)}[T_D]^{(e)}[K]^{-1}\begin{bmatrix} N^T \\ M^T \end{bmatrix} \tag{28}$$

IV. Results

A. Thermal Force Resultant and Moment For verification of the effectiveness of the analytical models, consider a corrugated-core sandwich panel unit cell with the following dimensions: a = 60 mm, h = 120 mm, e_{ms} = 1.5mm, e_n = 1.5 mm and $\theta = 65^o$. In the example the properties of the graphite/epoxy composite are assumed to be that of AS/Epoxy AS/3501, $E1$ = 140 GPa, $E2$ = 8 GPa, $G12$ = 7 GPa, =14, $\upsilon = 0.3$), The web and the face sheets are assumed to contain four laminas with the stacking sequence $[0/90]_2$. The representative volume element or unit cell used in the homogenization is shown in Fig. 8.

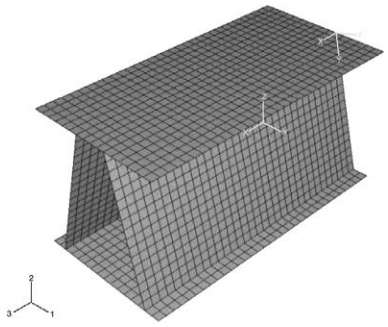

Figure 8. Finite Element Model

A finite element analysis was conducted on the unit cell using the commercial ABAQUSTM finite element program. Eight node shell elements were used to model the face sheets and the webs. The shell elements have the capability to include multiple layers of different material properties and thickness. Three integration points were used through the thickness of the shell elements. The FEM model consisted of 6600 nodes and 2160 elements. Known strains and curvatures were imposed on the unit cell. The force and moment resultants were calculated from the resulting stresses after the analysis. Strains were imposed by enforcing periodic displacement boundary conditions on the unit cell as shown in Table 1. To prevent rigid body motion and translation, the unit cell (Fig.9) was subjected to minimum support constraints.

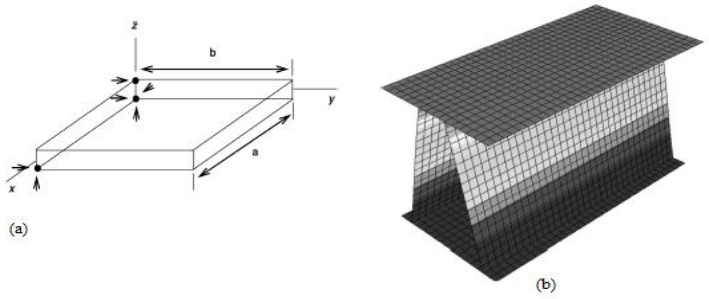

Fig. 9 a) Boundary Conditions imposed on the Pate. An arrow pointing at a Black Dot indicates that the Displacement of that Point is Fixed in the Direction of the Arrow. b) Deformation of the Unit Cell due to Temperature Distribution with the Unit Cell (Fully Constrained).

The top and bottom surfaces were assumed to be free of traction. The faces x=0 and x = *a* have identical nodes on each side as well as the other faces *y* = 0 and *y* = *b*. The identical nodes on the opposite faces are constrained to enforce the periodic boundary conditions. Figure 9 shows the deformations of the unit cell as a result of imposing the periodic boundary conditions.
The strains and curvature in Table 1 are set to zero to prevent expansion of the unit cell in the *x* and *y* direction. The 450s temperature distribution (Fig. 4a) was imposed on the FE model. The resulting force and moment resultant needed to constrain the unit cell when subjected to a temperature distribution will be equal to the negative of the thermal forces.

Table 1 Periodic Displacement Boundary Conditions imposed on the lateral faces of unit cell for in-plane strains and curvatures

$u(a,y)-u(0,y)$	$v(a,y)-v(0,y)$	$w(a,y)-w(0,y)$	$u(x,b)-u(x,0)$	$v(x,b)-v(x,0)$	$w(x,b)-w(x,0)$	$\theta_x(a,y)-\theta_x(0,y)$	$\theta_y(a,y)-\theta_y(0,y)$	$\theta_x(x,b)-\theta_x(x,0)$	$\theta_y(x,b)-\theta_y(x,0)$
$a\varepsilon_{x0}+az\kappa_x$	$a/2\gamma_{xy0}+az/2\kappa_{xy}$	$-a^2/2\kappa_x-ay/2\kappa_{xy}$	$b/2\gamma_{xy0}+bz/2\kappa_{xy}$	$b\varepsilon_{y0}+bz\kappa_y$	$-b^2/2\kappa_y-bx/2\kappa_{xy}$	$-a/2\kappa_{xy}$	$a\kappa_x$	$-b\kappa_y$	$b/2\kappa_{xy}$

The nodal forces of the boundary nodes were determined from the stress finite element output after the analyses. Then the force and moment resultants acting on the unit cell were obtained from the nodal forces using Eq. (29). The resultants obtained are the forces needed to constrain the unit cell, and they will be equal to the negative of the thermal forces. The results are shown in Table 2

Table 2 Non-zero thermal forces in the unit cell due to thorough thickness temperature distribution

	N_x, N/m	N_y, N/m	M_x, N m/m	M_y, N m/m
Analytical	581.03	317.48	10.97	11.41
Finite element	563.88	316.77	11.48	11.45
% diff.	3.04%	0.22%	4.36%	0.38%

$$[N_i, M_i] = \left(\frac{1}{b}\right) \sum_{m=1}^{n} [1, z] F_i^{(m)}(a, y, z) \tag{29}$$

The finite element results in Table 2 indicate that the maximum difference between exact thermal forces and those predicted by Eqs. (11–14) is less than 7% difference

B. Thermal Stress Verification

1. Constrained Case
Consider the same FEM unit cell representative volume element and mesh from Fig. 9 with the same material properties and cross ply layup. All strains in the *x* direction are zero and all strains in the *y*direction are zero for the unit cell (Table 1). The unit cell was subjected to the 450 s temperature distribution that was illustrated in Fig. 4a. The web was allowed to expand by the addition of rollers as shown in Fig. 5a. The strains in the webs were extracted from the finite element output after analysis. Figure 10 compares the finite element and analytical results for web strains

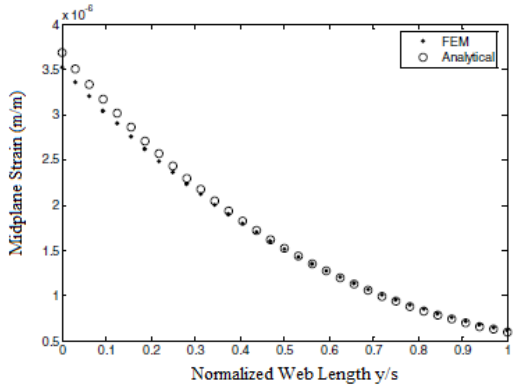

Fig. 10 Web strain expansion for the constrained thermal problem.

The results in Fig. 11 indicate that the analytical procedure developed to obtain the strain in the _ *y* direction, which accounts for the free expansion of the webs [Eqs. (19)nd (26] yields a less than 3% ifference strain result when compared with the FE results, which yield less than 7 %tress results when compared with finite element results, Fig. 12. Correct strain results are necessary to obtain accurate stress results.

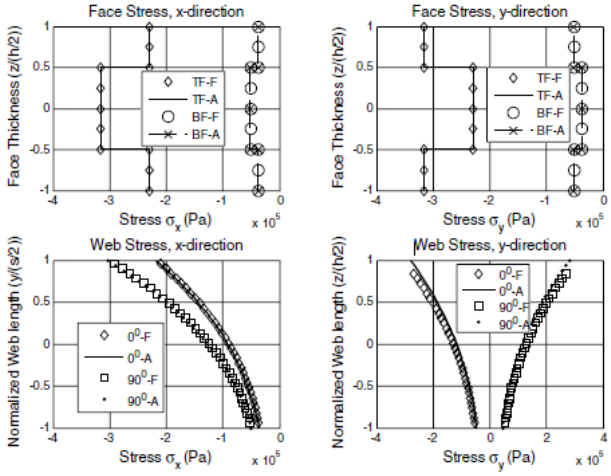

Fig. 12 Stresses in the x and y directions in the top face, bottom face, and web for the constrained thermal problem. A represents analytical results and F represents finite element results. The 0 and 90 indicate the ply orientation.

V. Conclusions

The truss-core sandwich panel, which is a candidate structure for ITPS, is homogenized as an equivalent orthotropic plate. Detailed formulation of the bending, extensional, coupling, and shear stiffness for an ITPS unit cell was presented. The ITPS will experience extreme reentry temperatures that will result in thermal moments and force resultants on the ITPS unit cell. A micromechanics approach was developed to determine unit-cell thermal forces and moments. The analytical model can be used to determine thermal forces and moments for the ITPS unit cell, which can lead to accurate thermal strains and stress. The results between finite element analysis and the analytical model for the constrained and unconstrained thermal problem were within 7% of each other, thus validating the method.

References

[1] Tan, K. H., Fung, T. C., and Lok, T. S., "A Simplified Thick Plate Analysis of All-Steel Sandwich Panels," Journal of Structural Engineering, Vol. 71, No. 14, 1993, pp. 253–258.
[2] Bapanapalli, S. K., Martinez, O., Sankar, B. V., Haftka, R. T., and Blosser, M. L., "Analysis and Design of Corrugated-Core Sandwich Panels for Thermal Protection Systems of Space Vehicles," 47th AIAA/ ASME/ASCE/AHS/ASC Structures, Structural Dynamics, and Materials Conference, AIAA, Reston, VA, May 2006.
[3] Fung, T. C., Tan, K. H., and Lok, T. S., "Analysis of *C*-Core Sandwich Plate Decking," Proceedings of the 3rd International Offshore and Polar Engineering Conference, International Society of Offshore and Polar Engineers, Republic of Singapore, Vol. 4, 1993, pp. 244–249. [14] Fung, T. C., Tan, K. H., and Lok, T. S., "Elastic Constants for *Z*-core sandwich panels," Journal of Structural Engineering, ASCE, Vol. 120, No. 10, 1994, pp 3046–3065. doi:10.1061/(ASCE)0733-9445(1994)120:10(3046)
[4] Libove, C. and Hubka, R. E., "Elastic Constants for Corrugated Core Sandwich Plates," National Advisory Committee for Aeronautics, Technical Note (NACATN)-2289, 1951.
[5] Vinson, J. R., The Behavior of Sandwich Structures of Isotropic and Composite Materials, Technomic, Lancaster, PA, 1999.
[6] Whitney, M., Structural Analysis of Laminated Anisotropic Plates, Technomic, Lancaster, PA, 1987.
[7] Martinez, O., Sankar, B. V., Haftka, R., Blosser, M., and Bapanapalli,S. K., "Micromechanical Analysis of a Composite Corrugated-Core Sandwich Panel for Integral Thermal Protection Systems," AIAA Journal, Vol. 45, No. 9, pp. 2323–2336. doi:10.2514/1.26779
[8] Blosser, M. L., "Advanced Metallic Thermal Protection Systems for Reusable Launch Vehicles," Ph.D. Dissertation, Mechanical and Aerospace Dept., Univ. of Virginia, Charlottesville, VA, 2000.

[9] Dorsey, J. T., Poteet, C. C., Wurster, K. E., and Chen, R. R., "Metallic Thermal Protection System Requirements, Environments, and Integrated Concepts," Journal of Spacecraft and Rockets, Vol. 41, No. 2, March–April 2004, pp. 162–172. doi:10.2514/1.9173
[10] Hibbeler, R. C., Mechanics of Materials, 4th ed., Prentice Hall, Upper Saddle River, NJ, 1999, p. 705.

Appendix

The transformation matrix for the top face sheet is

$$\{D\}^{(1)} = T_D^1 \{D\}^M$$

$$\begin{Bmatrix} \varepsilon_{xo} \\ \varepsilon_{yo} \\ \gamma_{xyo} \\ \kappa_x \\ \kappa_y \\ \kappa_{xy} \end{Bmatrix}^{(1)} = \begin{bmatrix} 1 & 0 & 0 & \frac{d}{2} & 0 & 0 \\ 0 & 1 & 0 & 0 & \frac{d}{2} & 0 \\ 0 & 0 & 1 & 0 & 0 & \frac{d}{2} \\ 0 & 0 & 0 & 1 & 0 & 0 \\ 0 & 0 & 0 & 0 & 1 & 0 \\ 0 & 0 & 0 & 0 & 0 & 1 \end{bmatrix} \begin{Bmatrix} \varepsilon_{xo} \\ \varepsilon_{yo} \\ \gamma_{xyo} \\ \kappa_x \\ \kappa_y \\ \kappa_{xy} \end{Bmatrix}^{(M)} \tag{A1}$$

The transformation matrix for the bottom face sheet is

$$\{D\}^{(2)} = T_D^2 \{D\}^M$$

$$\begin{Bmatrix} \varepsilon_{xo} \\ \varepsilon_{yo} \\ \gamma_{xyo} \\ \kappa_x \\ \kappa_y \\ \kappa_{xy} \end{Bmatrix}^{(1)} = \begin{bmatrix} 1 & 0 & 0 & -\frac{d}{2} & 0 & 0 \\ 0 & 1 & 0 & 0 & -\frac{d}{2} & 0 \\ 0 & 0 & 1 & 0 & 0 & -\frac{d}{2} \\ 0 & 0 & 0 & 1 & 0 & 0 \\ 0 & 0 & 0 & 0 & 1 & 0 \\ 0 & 0 & 0 & 0 & 0 & 1 \end{bmatrix} \begin{Bmatrix} \varepsilon_{xo} \\ \varepsilon_{yo} \\ \gamma_{xyo} \\ \kappa_x \\ \kappa_y \\ \kappa_{xy} \end{Bmatrix}^{(M)} \tag{A2}$$

The transformation matrix for the left web is

$$\{D\}^{(e)} = T_D^e \{D\}^M \qquad \begin{Bmatrix} \varepsilon_{\bar{x}o} \\ \varepsilon_{\bar{y}o} \\ \gamma_{\bar{x}\bar{y}o} \\ \kappa_{\bar{x}} \\ \kappa_{\bar{y}} \\ \kappa_{\bar{x}\bar{y}} \end{Bmatrix}^{(3)} = \begin{bmatrix} 1 & 0 & 0 & (\frac{d_c}{2} - \bar{y}\sin\theta) & 0 & 0 \\ \nu & 0 & 0 & \nu(\frac{d_c}{2} - \bar{y}\sin\theta) & 0 & 0 \\ 0 & 0 & -f(p,d,t_{TF},t_{BF},t_w,\theta) & 0 & 0 & 0 \\ 0 & 0 & 0 & -\cos\theta & 0 & 0 \\ 0 & 0 & 0 & 0 & -g(p,d,t_{TF},t_{BF},t_w,\theta) & 0 \\ 0 & 0 & 0 & 0 & 0 & 1 \end{bmatrix} \begin{Bmatrix} \varepsilon_{xo} \\ \varepsilon_{yo} \\ \gamma_{xyo} \\ \kappa_x \\ \kappa_y \\ \kappa_{xy} \end{Bmatrix}^{(M)} \tag{A3}$$

The transformation matrix for the right web is

$$\{D\}^{(e)} = T_D^e \{D\}^M \qquad \begin{Bmatrix} \varepsilon_{\bar{x}o} \\ \varepsilon_{\bar{y}o} \\ \gamma_{\bar{x}\bar{y}o} \\ \kappa_{\bar{x}} \\ \kappa_{\bar{y}} \\ \kappa_{\bar{x}\bar{y}} \end{Bmatrix}^{(3)} = \begin{bmatrix} 1 & 0 & 0 & (\frac{d_c}{2} - \bar{y}\sin\theta) & 0 & 0 \\ \nu & 0 & 0 & \nu(\frac{d_c}{2} - \bar{y}\sin\theta) & 0 & 0 \\ 0 & 0 & f(p,d,t_{TF},t_{BF},t_w,\theta) & 0 & 0 & 0 \\ 0 & 0 & 0 & -\cos\theta & 0 & 0 \\ 0 & 0 & 0 & 0 & g(p,d,t_{TF},t_{BF},t_w,\theta) & 0 \\ 0 & 0 & 0 & 0 & 0 & 1 \end{bmatrix} \begin{Bmatrix} \varepsilon_{xo} \\ \varepsilon_{yo} \\ \gamma_{xyo} \\ \kappa_x \\ \kappa_y \\ \kappa_{xy} \end{Bmatrix}^{(M)} \tag{A4}$$